Wear 368-369 (2016) 75–83

Contents lists available at ScienceDirect

Wear

journal homepage: www.elsevier.com/locate/wear

Effect of surface films on tribologically induced metallurgical transformations of steel in oil lubricated contacts

Shoufan Cao [a,*], François Sarasin [b], Marco Cantoni [c], Stefano Mischler [a]

[a] Ecole Polytechnique Fédérale de Lausanne (EPFL), Tribology and Interface Chemistry Group, Station 12, CH-1015 Lausanne, Switzerland
[b] Micro Tech Lubes SA, 1207 Geneva, Switzerland
[c] Ecole Polytechnique Fédérale de Lausanne (EPFL), Interdisciplinary Center for Electron Microscopy (CIME), Station 12, CH-1015 Lausanne, Switzerland

ARTICLE INFO

Article history:
Received 31 May 2016
Received in revised form
9 August 2016
Accepted 8 September 2016
Available online 14 September 2016

Keywords:
Wear
Tribological transformation of surface (TTS)
Subsurface deformation
Plastic flow
Boundary films

ABSTRACT

This study was initiated with the aim to assess the influence of boundary films on the tribologically induced metallurgical transformations and deformations of metals in lubricated contacts and their effect on wear. For this, the tribological behavior of a carbon steel contact was studied in two commercially available oils expected to form boundary films of quite different chemistry and structure. Surface analysis by AES and XPS revealed that under the investigated conditions the first oil led to the formation of an iron–zinc oxide surface film while the second to a calcium–carbon–oxygen rich film. The results show that, without influencing the coefficient of friction, the nature of the formed films significantly affected the metallurgical transformations (characterized by electron microscopy of focused ion beam cross sections) occurring in the near surface region of the metal and the corresponding wear response. The effect of boundary films on wear was attributed to their capability to influence the plastic flow of the nano-grained structures generated in the studied tribological contacts.

1. Introduction

Anti-wear additives used in oil lubricants are designed to generate, by chemical reaction, surface films acting as boundary lubricants to protect the underlying metal against wear. One of the most studied anti-wear additives for oil is the family of ZDDP (zinc dialkyl-dithiophosphate), which is effective under a variety of tribological conditions [1,2]. ZDDP forms boundary films of complex structure that may include several layers: a metal oxide or sulfide layer interfacing the metal, a layer of short chain phosphates, a layer of long chain poly(thio)phosphates and finally with a soft surface layer of alkyl phosphates [2]. Other additives react differently. For example, Minami et al. [3] reported that over-based calcium sulfonates introduced into base oil generated an efficient wear protective boundary film composed of $CaCO_3$ and CaO.

It is generally accepted that anti-wear boundary films constitute a mechanical protective barrier that acts by different mechanisms. Their effectiveness is usually attributed to their low shear strength that reduces friction and to their capability to avoid direct metal on metal contact, thus preventing adhesion, and to digest hard abrasive particles [1,2].

However, other mechanisms can in principle play a role. Surface films can affect the tribological behavior of metals by directly interfering with the plastic deformation mechanism of metals. Indeed, surface oxide films were observed to render certain metal more brittle and thus more prone to wear. This effect was first observed in the early 20th century by Roscoe [4] who investigated the mechanical properties of cadmium oxidized at different levels. Recently, in water lubricated contacts (tribocorrosion) passive films, i.e. nanometer thin oxide surface films spontaneously formed by reaction of the metal with water, were found to promote strain accumulation in the near surface zone of rubbed metals such as carbon steel [5], stainless steel [6], CoCr alloys [7] and NiCr alloys [8] and to promote wear. The strain accumulation manifested itself in hardening and in extended grain refinement leading to the formation of nano-sized grains in the near surface metal layer [6–8]. As a consequence of strain accumulation, the material became more prone to mechanical failure and wear than the same metal without the passive film. This tribo-metallurgical effect was tentatively attributed to the blocking action that surface films can have on dislocation motion and their annihilation at the surface [6,9]. Büscher et al. [10] found that during the rotation of the nano-grains in the near surface zone under the frictional stress field, surface active species can react with the exposed grain boundaries and thus reduce intergranular adherence and overall surface cohesion resulting in enhanced wear.

* Corresponding author.
E-mail address: shoufan.cao@epfl.ch (S. Cao).

http://dx.doi.org/10.1016/j.wear.2016.09.011
0043-1648/

This work was initiated with the aim to verify whether surface films generated on steel in oil lubricated contacts may indeed modify the tribo-metallurgical response to friction. For this, a bearing ball vs. carbon steel disc contact was evaluated in a reciprocating sliding wear rig lubricated using two different oils. The first one is a fully formulated commercial oil containing among other additives ZDDP (zinc dialkyl-dithiophosphate). In order to modify the nature of the boundary film without affecting the other oil properties, a fully miscible commercial calcium sulfonate and PAO (poly alpha olefin) based additive package was added to the first oil to form the second oil. According to literature [1–3], these two lubricants are supposed to produce boundary films of different nature. Although these lubricants are specifically designed as engine oil for higher temperatures, tribological tests were carried out at room temperature, the goal of this study being comparing different boundary films, not testing the efficiency of oil formulations. Surface chemistry was assessed using Auger Electron Spectroscopy (AES) and X-ray Photoelectron Spectroscopy (XPS). Focused Ion Beam (FIB) cross sections were analyzed by Scanning Electron Microscopy (SEM) to reveal metallurgical transformations induced by rubbing in the near surface region.

2. Experimental

2.1. Materials and lubricants

Disks of 20 mm diameter and 5 mm thickness made of 1.6582 carbon steel (V155 from Böhler Steel, Austria) were used as flat samples. The chemical composition is 0.34% C, 1.5% Cr, 1.5% Ni, 0.2% Mo, 0.5% Mn, 0.3% Si and balance Fe. According to the manufacturer, the V155 steel is delivered in tempered state with yield strength of 900 MPa. Fig. 1 shows the metallurgical structure of the metal used for the disks. A very fine and homogeneous annealed martensitic structure was found. The balls, with diameter of 6 mm, were made of 1.3505 bearing steel (100Cr6 from Bossard AG, Zug/Switzerland). According to the supplier, the surface roughness of the bearing balls is 60 nm. The disks were polished down to mirror grade. Prior to tests, the balls and disks were ultrasonically cleaned in acetone and ethanol for 5 min respectively and dried with oil free compressed air.

The oil used was an industrial fully synthetic motor oil (Mobil 1 0W-40), hereinafter referred to as “Oil A”. The PAO/calcium sulfonate additive package Engine Treatment commercialized by BestLine Research Inc. was blended with Oil A (15 vol%) in order to obtain the second lubricant called hereinafter “Oil B”. According to the manufacturers, the Oil A contains 1100 ppm of zinc and the additive package contains group III and group IV PAOs (including aliphatic spirits, 1-decene hydrocarbon and cycloparaffins), liquid fluorocarbon resins and synthetic antioxidant calcium sulfonates. Both the oil and the additive package were supplied by Micro Tech Lubes SA (Geneva, Switzerland). The viscosity of Oil A and B was measured at room temperature (22 ± 1 °C) using a viscometer (Model RI:1:L from Rheology International Shannon, Ireland). Spindle 2 was used and five rotating speeds (20, 30, 50, 60, 100 rpm) were applied to obtain the viscosity, respectively. At the above different rotating speeds, no big difference of the viscosity was found. The viscosity of the Oil A is 171 ± 2 mPa · s and the Oil B has a very close viscosity of 169 ± 1 mPa · s.

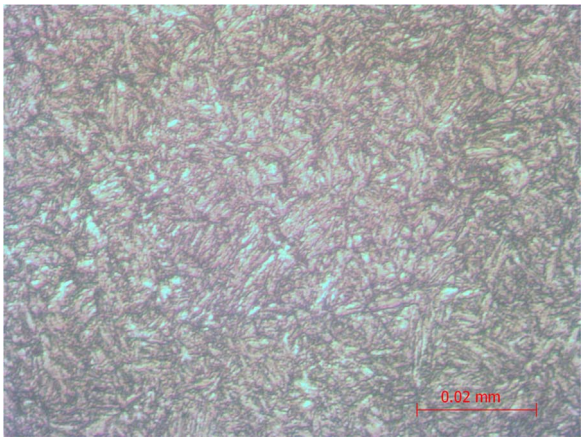

Fig. 1. The metallurgical structure of the metal (V155) used for the disks.

Table 1
Experimental parameters of the wear tests.

Motion	Reciprocating
Load	3.9 N or 5.7 N
Average Hertzian contact pressure	692 MPa or 785 MPa
Stroke length	5 mm
Frequency	4 Hz
Sliding velocity	40 mm/s

2.2. Tribology tests

Ball-on-disc configuration was adopted to carry out the tribology tests. The reciprocating motion tribometer used is described in more details in [11,12]. Before sliding, the loaded ball and disc were left in the lubricant for 5 min. Then the sliding started and lasted for 120 min. After sliding, the loaded ball and disc were left in the lubricant for another 5 min. Table 1 shows the experimental parameters for the tests. The coefficient of friction was recorded during the whole rubbing period as the ratio between the frictional and normal force when the ball was in the middle of the stroke. After the test, the disc and the ball were ultrasonically cleaned first in petrol and then in ethanol for 10 min, respectively and dried by compressed air.

2.3. Characterization

The topography of wear tracks was observed under optical microscope (Leitz), SEM (Phillips XLF30) and 3D white light interferometer (GBS smartWLI). The volume of the wear track on the disc was calculated by multiplying the area of the cross section of the wear track by its length.

Micro-hardness was measured using a Vickers micro hardness tester (Leitz) inside and outside of the wear tracks. Average values were calculated from five individual tests. The applied load was 0.98 N and the dwell time was 15 s.

Cross section images of the wear tracks (perpendicular to the sliding direction) were obtained from serial high-resolution SEM images in a combined FIB-SEM system (Zeiss XB540). A Ga^+ ion beam was used in the FIB system to mill the cross section surfaces. 3D reconstruction was implemented using an open-source image processing software (Fiji). 300 cross section images at 10 nm spacing obtained from the FIB system were employed and then aligned and segmented by Fiji. The plugin “3D Viewer” was used to acquire the 3D images.

The chemical composition of the surfaces (inside and outside of the wear track) after the wear tests was analyzed by AES and XPS. AES was carried out using a PHI 680 Scanning Auger Microscope (Physical Instruments AG, Germany) operated with a primary beam of 10 nA at 10 keV. AES sputtering depth profiles were measured using a 1 keV Ar^+ ion beam rastered over an area of 2×2 mm corresponding to a sputtering rate of 2 nm/min as calibrated on SiO_2 films. XPS measurements were carried out using a

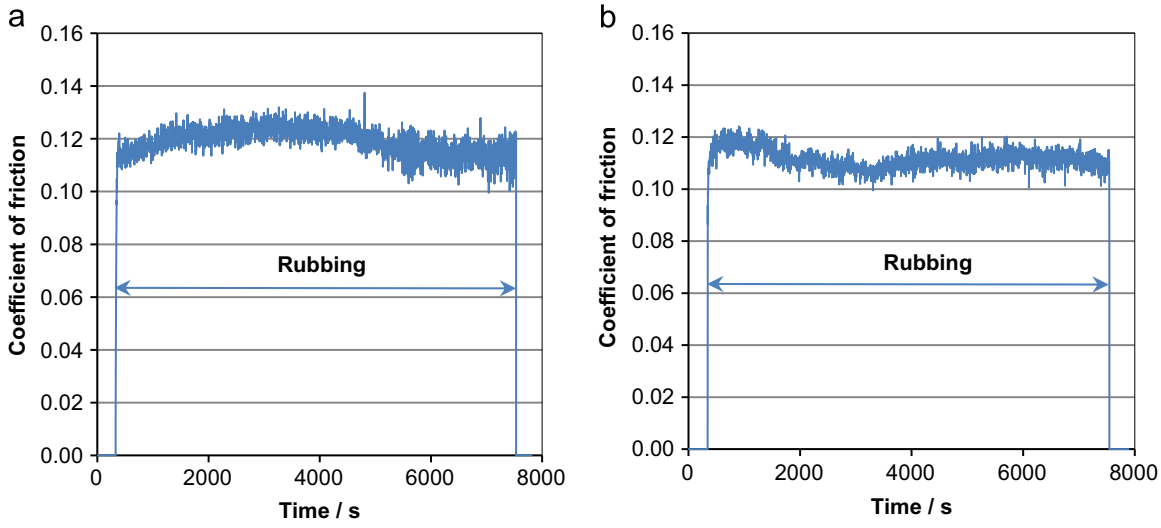

Fig. 2. Typical coefficient of friction curve in Oil A (a) and Oil B (b). Normal load: 5.7 N.

Table 2
Average coefficient of friction (COF) and wear volumes of the wear tracks.

Test	Load (N)	COF	V_{below} (10^{-3} mm^3)	V_{above} (10^{-3} mm^3)	V_{wear} (10^{-3} mm^3)
In Oil A	3.9	0.14	1.48 ± 0.62	0.03 ± 0.01	1.45 ± 0.55
		0.13	0.47 ± 0.23	0.01 ± 0.01	0.46 ± 0.23
		0.13	1.02 ± 0.53	0.03 ± 0.01	0.99 ± 0.49
	5.7	0.12	3.00 ± 0.87	0.04 ± 0.02	2.96 ± 0.82
		0.12	1.81 ± 0.62	0.03 ± 0.01	1.78 ± 0.61
		0.13	1.63 ± 0.34	0.01 ± 0.005	1.62 ± 0.34
In Oil B	3.9	0.11	0.06 ± 0.03	0.01 ± 0.003	0.05 ± 0.02
		0.12	0.07 ± 0.05	0.01 ± 0.005	0.06 ± 0.03
		0.11	$0.05 + 0.04$	$0.01 + 0.005$	0.04 ± 0.02
	5.7	0.12	0.06 ± 0.02	0.02 ± 0.004	0.04 ± 0.02
		0.11	0.06 ± 0.02	0.02 ± 0.009	0.04 ± 0.03

PHI Versa Probe II scanning XPS microprobe (Physical Instruments AG, Germany). Analysis was performed using a monochromatic Al Kα X-ray source of 24.8 W power with a beam size of 100 μm in diameter. Binding energies were calibrated by setting the carbon 1 s peak position at 284.8 eV.

3. Results

3.1. Coefficient of friction

The friction coefficient tested in Oil A varies between 0.1 and 0.13, as shown in Fig. 2. In Oil B, the same behavior is observed although friction is slightly lower (between 0.1 and 0.12). The values of the coefficient of friction averaged over the entire rubbing period are listed in Table 2 for each of the repetitions.

3.2. Wear loss

Fig. 3 shows two typical white light interferometry 3D images of the central section of the wear track formed in the two oils.

Fig. 3 clearly shows that the wear track formed in Oil A is significantly larger than the one formed in Oil B. The latter exhibits blunter ridges. Six profiles were taken perpendicularly to the sliding direction from the measured 3D profiles. Then the area below the baseline and above the baseline (set at the height of the non-rubbed surface) can be obtained from the six profiles, respectively. The average cross section area of the six profiles was multiplied by the length of the wear track in order to obtain the volume. The obtained volumes are listed in Table 2. The V_{below} is the volume of the wear track below the baseline and the V above is the volume of the generated ridges above the baseline. In this way, only the material effectively removed from the sample (V_{wear}) was considered as wear, $V_{wear} = V_{below} - V_{above}$. Wear volumes in Oil A scatter considerably and are larger at higher load. Wear volumes obtained in Oil B are more than one order of magnitude smaller compared to Oil A. This wear reducing effect is more pronounced at higher load. Interestingly, load seems to have little or no effect on wear in Oil B.

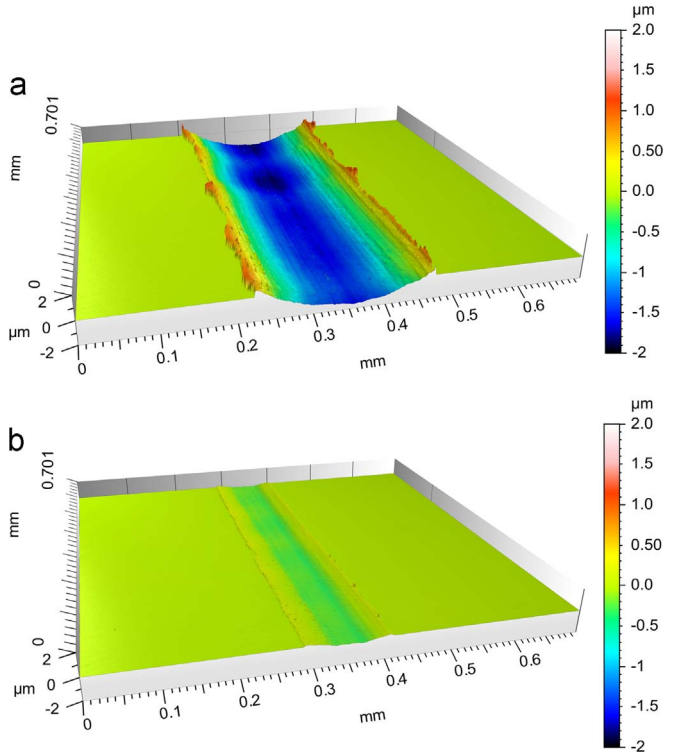

Fig. 3. 3D image of the wear track on the disc from tests in Oil A (a) and in Oil B (b) as measured using the white light interferometer. Normal load: 5.7 N.

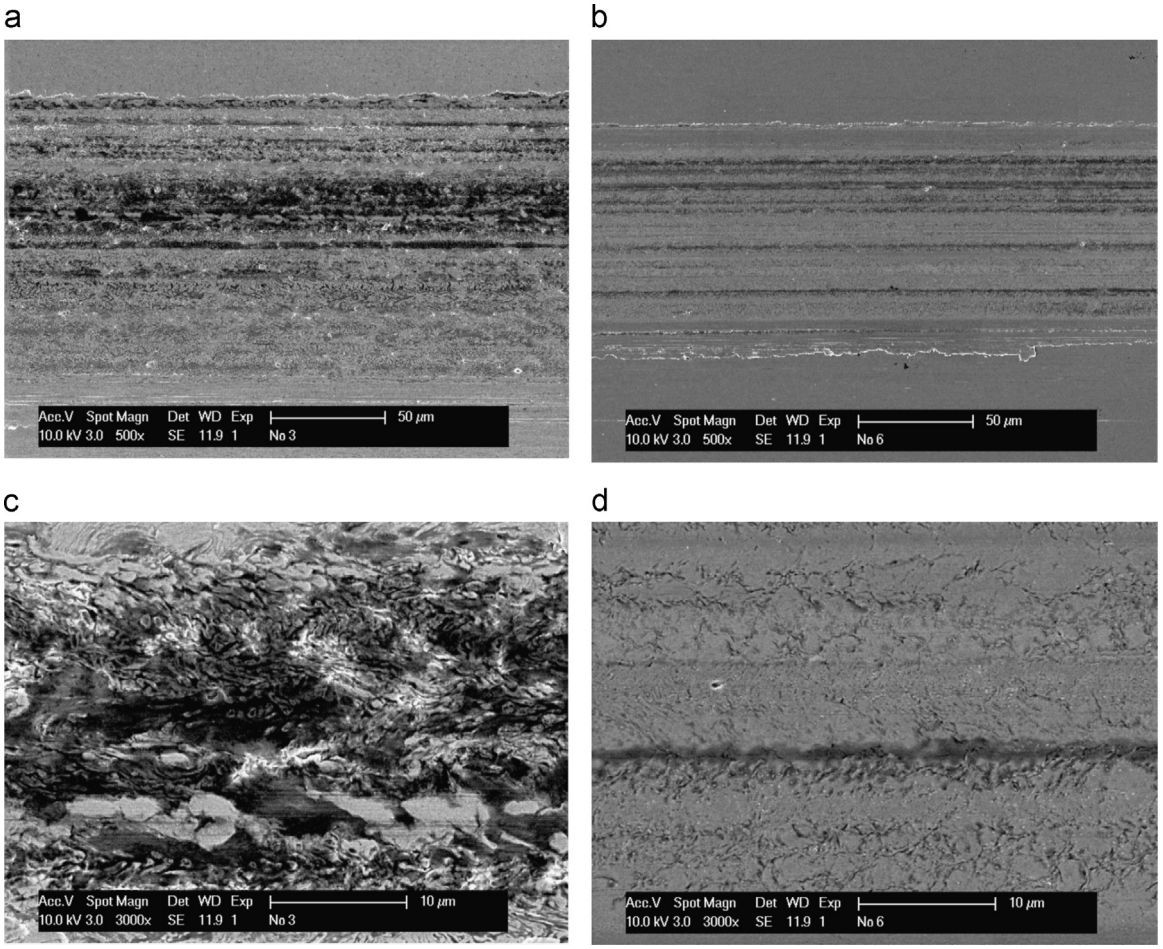

Fig. 4. SEM images of the wear tracks on the disks rubbed in Oil A (a and c) or Oil B (b and d). Normal load: 3.9 N.

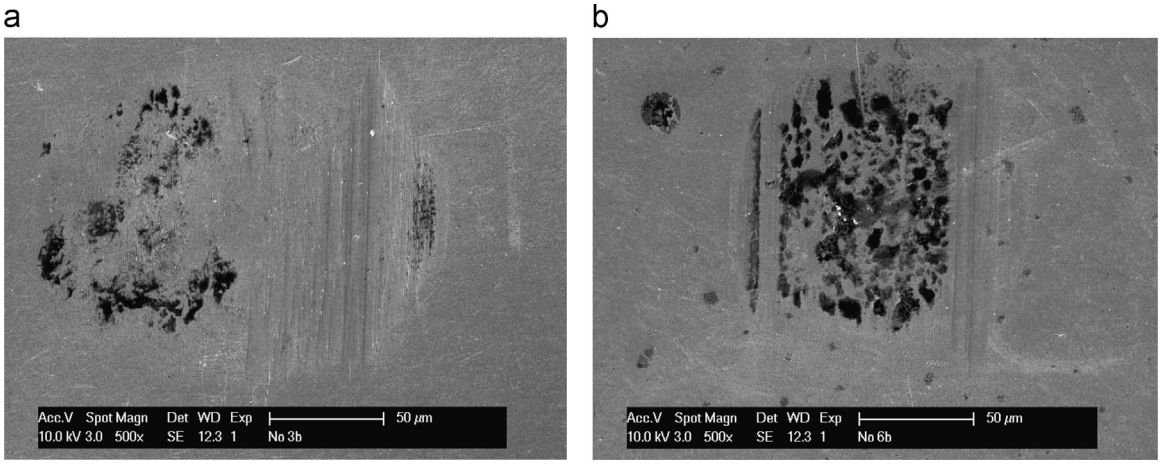

Fig. 5. SEM images of the wear scars on the balls rubbed in Oil A (a) or Oil B (b). Normal load: 3.9 N.

3.3. *Worn area topography*

Fig. 4 shows typical SEM images of the wear tracks generated on the disks. The ridges, the disrupted appearance of the surface and the scratches aligned to the sliding direction (left to right) indicate the occurrence of plastic deformation. The wear track formed in Oil B is finer and more homogeneous. The same wear topography was found independently on the two applied loads.

The SEM images of the worn area of the balls are shown in Fig. 5. Scratches and damaged areas are visible on the balls. No large circular or elliptical wear scars can be observed in Fig. 5, which indicates absence of significant wear of the balls. However, some surface depressions or scratches, as confirmed by the white light interferometry in Fig. 6, can be observed indicating local ball material removal due probably to interactions with counter body asperities or third bodies. Noteworthy is that the dark spots (possibly material transfer) seems more pronounced in the case of tests carried out in Oil B. Similar patterns were found for both of the applied loads.

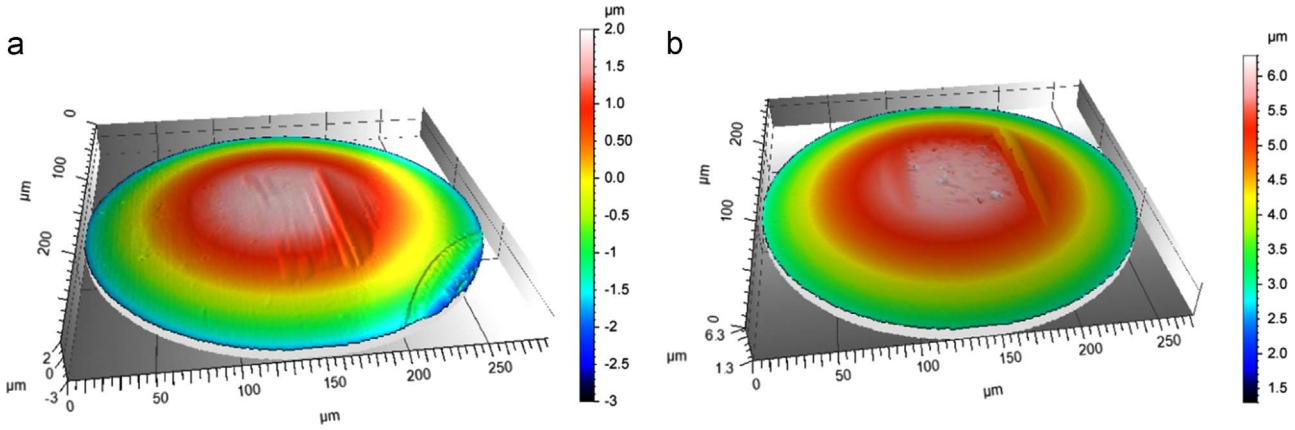

Fig. 6. 3D images of the wear scars presented in Fig. 5 in Oil A (a) or Oil B (b).

Table 3
Surface micro-hardness (load 0.98 N) measured outside and inside the wear tracks.

Test	Location	HV average[a] (3.9 N)	HV average[a] (5.7 N)
Test in Oil A	Outside	396 ± 10	397 ± 11
	Inside	479 ± 16	469 ± 16
Test in Oil B	Outside	386 ± 9	400 ± 6
	Inside	446 ± 6	437 ± 18

[a] Average and deviation from 5 independent measurements. Indentation depth ranged between 2.7 and 2.9 um.

3.4. Micro-hardness and FIB cross section

Table 3 shows the micro-hardness outside and inside of the wear tracks on the disks tested at the two loads. It can be seen that the tribological induced surface hardening in Oil A is larger than in Oil B. No significant differences can be observed between the two investigated loads for both oils.

FIB cross sections were carried out on samples tested at 3.9 N only. Fig. 7 shows the SEM images of the FIB cross section of the wear tracks. The gray contrast comes from the different orientations of the grains. A nano-crystalline layer was found underneath the wear surface in both lubricants, which results from recrystallization phenomena due to the plastic strain induced by friction. This nano-crystalline layer is approximately 4 µm thick in both lubricants. Differences between lubricants appear in the morphology. Some vortexes characterized by elongated and curved grains were found on the wear surface tested in Oil A. These vortexes may result from local flows due to the severe deformation of the wear surface. The near surface microstructure of the sample tested in Oil B is more homogeneous and free of any vortex or other discontinuity.

The 3D reconstructed images shown in Fig. 8(a) and (b) represents a solid cube of $3 \times 3 \times 3$ µm dimension taken inside the nano-crystalline layer from the worn surface. For the reconstruction, the grains close to a certain orientation (i.e. a well-defined gray level) were numerically isolated from the others and reconstructed in order to obtain the 3D images. In Fig. 8(a) and (b), they are presented in a 60° view with the upper part corresponding to the worn surface. Fig. 8(c) is one top view plane image sectioned from Fig. 8(a) at a depth of 0.5 µm from the worn surface and Fig. 8 (e) is obtained at 2 µm from the worn surface. Similarly, Fig. 8 (d) and (f) are obtained from Fig. 8(b) using the same method.

Fig. 8 shows clear differences in plastic response of the disc steel between the two lubricants. Clearly, in Oil A, the isolated grains are elongated along the sliding direction (Fig. 8a and c). This elongation is less pronounced below approximately 1 µm from the surface. The nano-grains formed in Oil B exhibit rather isotropic dimensions with no evident texturing along the sliding direction (Fig. 8b and d).

3.5. Surface chemical composition

The surfaces were analyzed using AES to obtain depth profiles by sputtering and using XPS to identify the chemical state of the elements. The wear tracks on the disks were analyzed by AES for both loads and similar depth profiles were found independently on the load in the same oil while significant differences were found between the two oils. For the balls, only the samples tested at 5.7 N were analyzed by XPS since a bigger wear scar facilitates identification of the area to be analyzed. As a result, in the following, the AES and XPS results from the samples tested at 5.7 N are presented.

Typical AES depth profiles taken inside of the wear tracks on the disks are shown in Fig. 9 (in Oil A) and Fig. 10 (in Oil B). Due to the non-uniform appearance of the wear track, depth profiles were simultaneously measured at different locations as shown in Figs. 9 and 10. Measurement repetition on second samples treated under the same conditions yielded similar results as shown in Figs. 9 and 10.

The surface worn in Oil A (Fig. 9b) exhibits a multilayered structure consisting of an outer calcium rich layer supported by an internal thicker layer containing mainly oxygen, iron, zinc and sulfur. The thickness of these layers varies locally: in Fig. 9b it is 150 nm thick (considering the 50% drop of the oxygen signal) while in Fig. 9c the thickness is only 95 nm. A weak phosphorus signal was detected only on the outermost surface and it disappeared after 2 min sputtering (corresponding to 4 nm).

As shown in Fig. 10, wear experiments in Oil B yield a quite different surface composition. Indeed, the worn surfaces appear covered by a layer composed mainly by calcium, oxygen and carbon. Only relatively small amount of iron was found in this layer. No zinc signals were detected. The thickness of this layer varies also between 10 nm (Fig. 10c) and 60 nm (Fig. 10b), which indicate the non-uniform coverage of this film on the metal surface.

AES depth profiling was performed for comparison on the areas outside of the wear track on the disks. The obtained profiles showed the presence of a 3–5 nm thin oxide layer typically formed on steel upon air exposure. No significant differences in composition of the steel surfaces between Oil A and B were found outside of the wear track.

The surfaces on the disks were then analyzed using XPS in order to identify the chemical states of the elements identified by AES analysis. In order to remove surface contaminations generated by exposure to air, the surfaces were sputter cleaned prior to

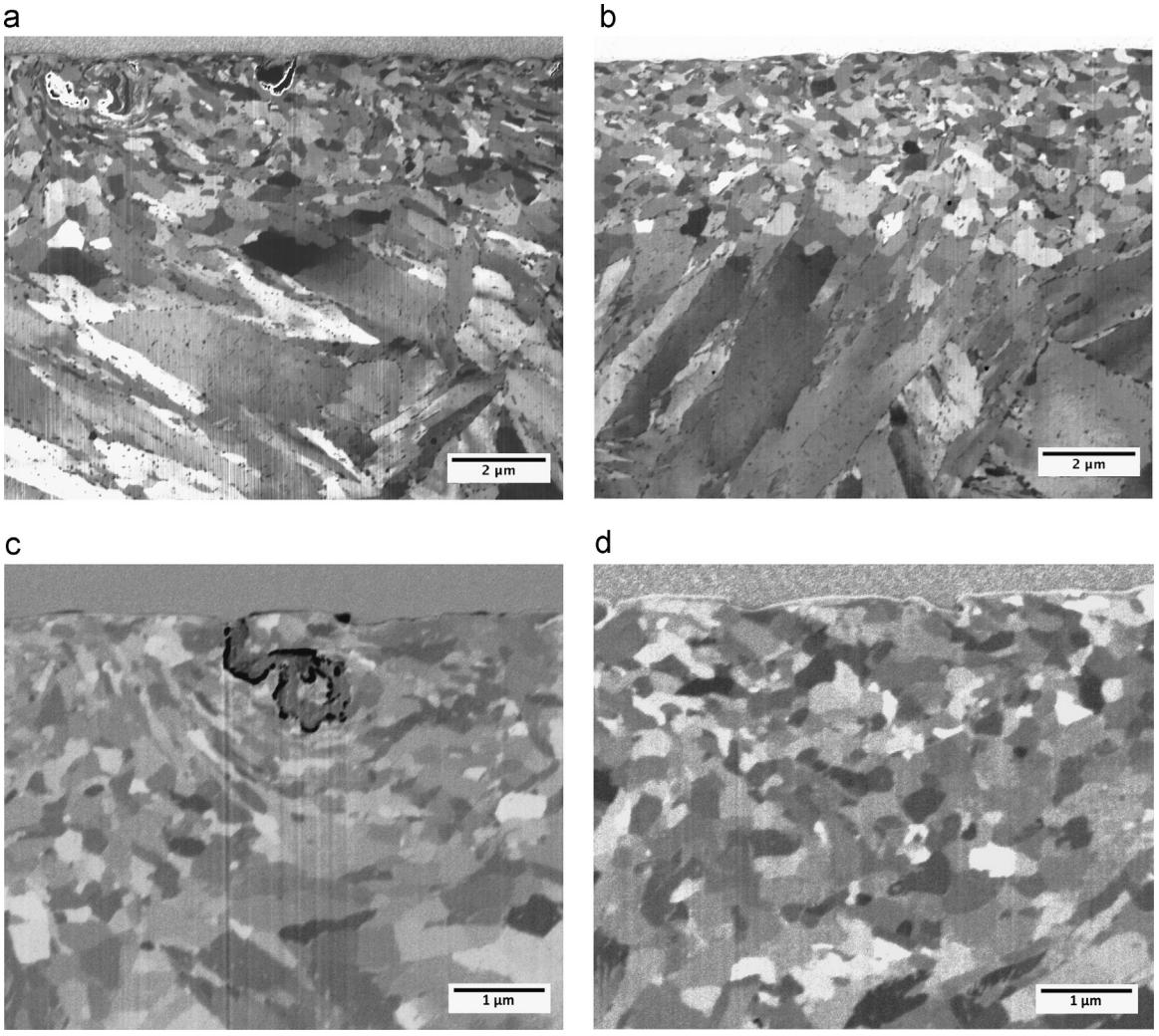

Fig. 7. FIB cross section images of the wear tracks on the disks rubbed in Oil A (a and c) and in Oil B (b and d). Normal load: 3.9 N, sliding direction: perpendicular to the image plane.

analysis with a 2 keV Ar^+ ion gun allowing the removal of approximately 5 nm material. The spectra showed the presence of the elements already identified in AES, i.e. Fe, Ca, Zn, S, P, C and O. Zn, P and S could be identified only in the surface worn in Oil A. Spectra were analyzed and compared using the data provided in the XPS handbook [13] and NIST (National Institute of Standards and Technology) XPS database [14]. A single peak of 710 eV binding energy corresponding to oxidized metal composed the Fe $2p_{3/2}$ spectrum in both oils. The binding energy of Zn $2p_{3/2}$ peak of 1021.6 eV and the Auger LMM kinetic energy of 498 eV indicated that zinc presented in its oxidized form. The Ca $2p_{3/2}$ peak was positioned for both oils at 347.1 eV corresponding to calcium oxide and/or carbonate. The binding energies of the sulfur and the phosphorus 2p peaks were 160.9 eV and 132.7 eV respectively, corresponding to sulfide and phosphate oxidation states. The O 1s signal showed clearly the presence of two peaks: one positioned at 531.4 eV (corresponding to hydroxide and/or phosphate and/or carbonate) and the second at 529.7 eV corresponding to metal oxide. The C 1 s signal also showed the presence of two peaks corresponding to different oxidation states: carbonate (288.7 eV) and C–H bonds (284.8 eV). No qualitative differences in O 1 s and C 1 s spectra could be revealed on samples worn in Oil A or B, only the relative intensity of the two contributions varied slightly.

The AES and XPS analysis indicate thus two different surface chemistries in Oil A and B. The calcium oxide or carbonate rich layer covering the surface rubbed in Oil B and presenting on the outermost surface of the film formed in Oil A is consistent with the reaction of calcium sulfonate [3], an additive presenting in Oil A and, in larger amounts, in Oil B. The formation of mixed iron–zinc oxide as observed in Oil A is typical for the reaction of ZDDP like additives [1,2]. The presence of sulfur and phosphorous on the surface lends support to the reactivity of ZDDP like additives. Interestingly, it seems that the additive package blended with Oil A to form Oil B suppresses the formation of the iron–zinc oxide film, i.e. it seems to hinder the reaction of ZDDP at least under the present experimental conditions.

The balls worn at 5.7 N were analyzed by XPS. Before sputtering, the XPS spectra exhibited regardless of lubricant the peaks of C, O, Cr and Fe with slight contamination of S and Ca that disappeared after sputtering. This indicates that no or very thin boundary films formed on the balls.

4. Discussion

The experimental results described above clearly show that wear is largely reduced in Oil B. The two lubricants yield boundary films that differ significantly in chemistry but provide the similar coefficient of friction (Table 2). Thus, the generally accepted friction reducing effect of low shear strength surface layers cannot

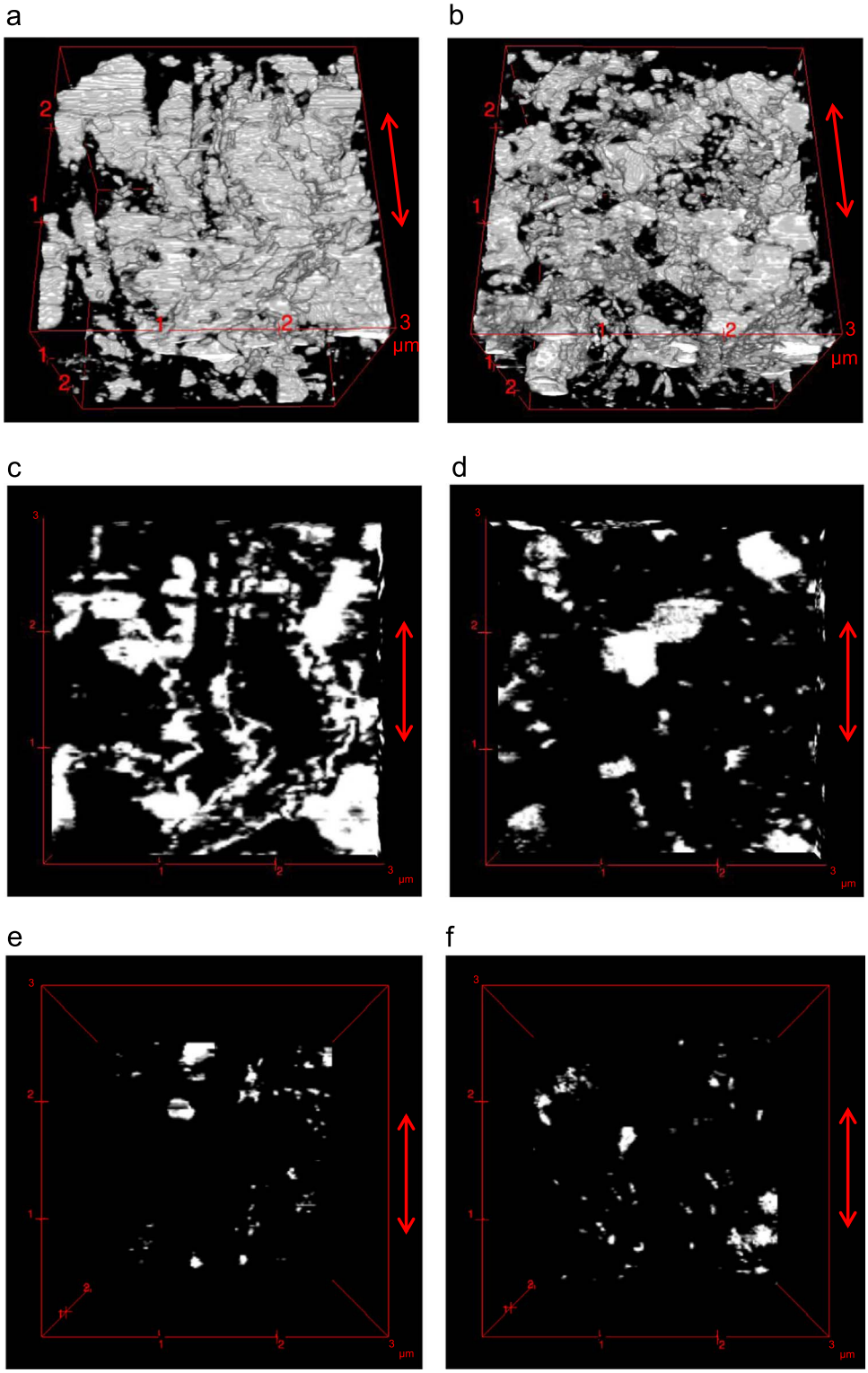

Fig. 8. Reconstructed images of the grain structure underneath the wear tracks on the disks rubbed in Oil A (a, c and e) and in Oil B (b, d and f). Normal force: 3.9 N, (a) and (b) are in 60° view, (c)–(f) are in top view, sliding direction is indicated by the arrows.

explain the observed differences in wear. Rather, the wear reducing effect is likely linked to other mechanisms that will be tentatively analyzed in the following.

In contacts characterized by chemical surface reactions between contacting material and environment, i.e. tribocorrosion situations [9], material removal from rubbing surfaces can proceed by the detachment of metal particles as well as of surface reaction films such as the boundary films found here.

A better mechanical stability of the boundary film formed in Oil B would contribute to limit wear with respect to Oil A. At present, it is not possible to measure the rate of boundary film removal and thus the impact on wear in Oil A and B of cyclic boundary film removal followed by its reconstitution cannot be assessed. Unfortunately oil is not an electrolyte and thus electrochemical techniques, successfully used to quantify in-situ and in real time this mechanism in aqueous solutions [5–9], are not applicable.

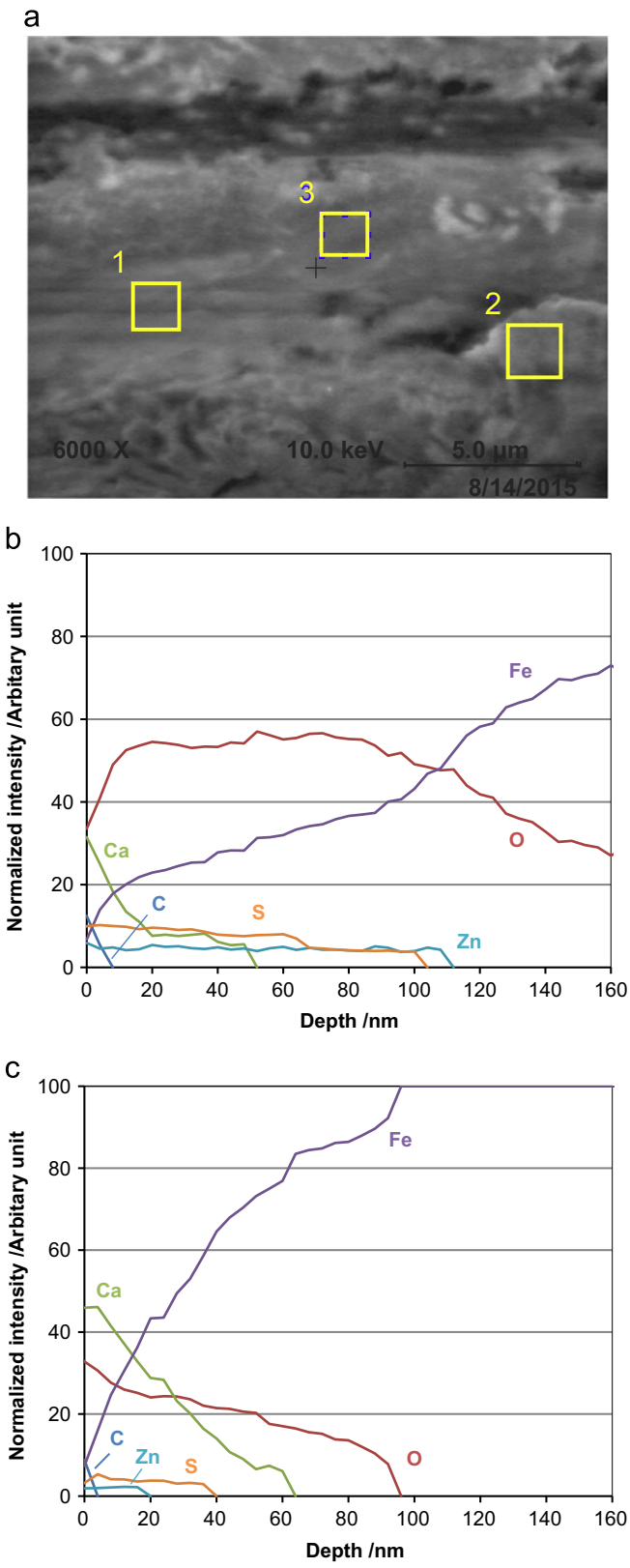

Fig. 9. SEM images and typical AES depth profiles inside the wear tracks on the disks rubbed in Oil A. Profile (b) corresponds to spots 1 (spot 3 has a similar profile) and profile (c) corresponds to spot 2 in (a). Normal force: 5.7 N.

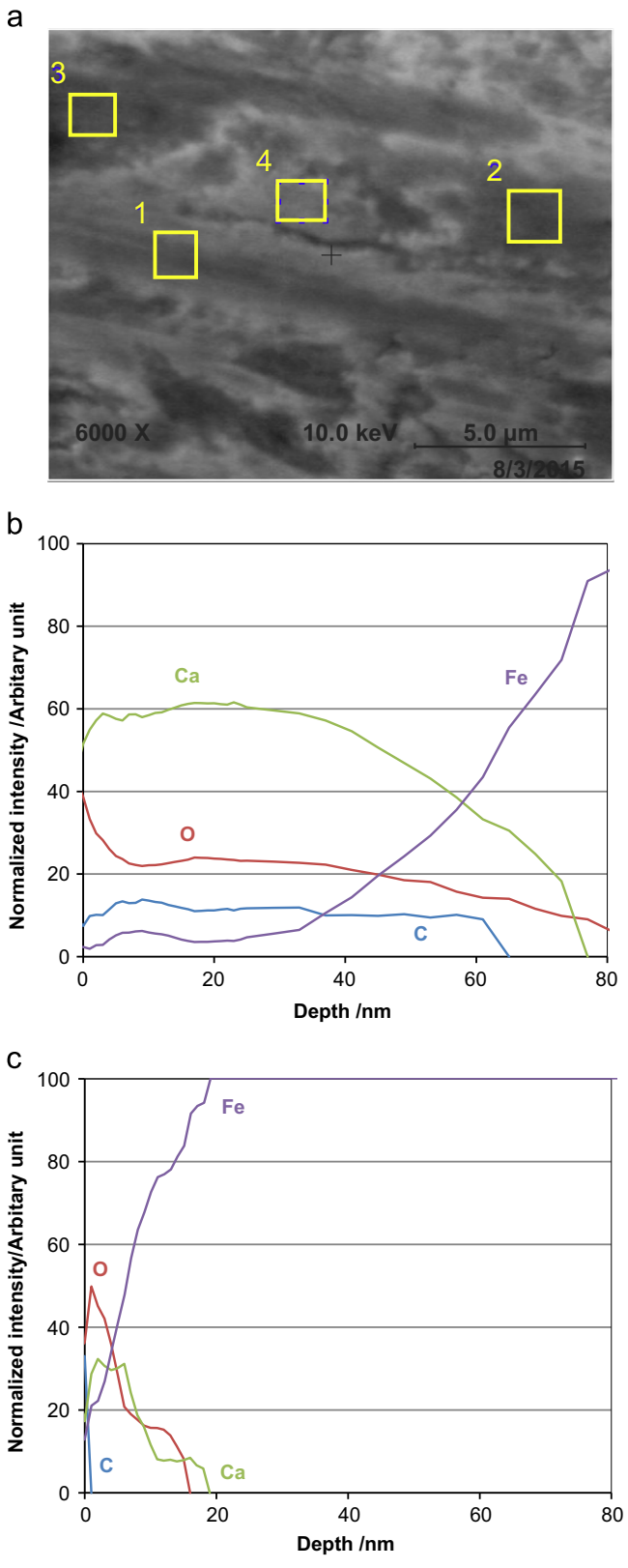

Fig. 10. SEM images and typical AES depth profiles inside the wear tracks on the disks rubbed in Oil B. Profile (b) corresponds to spot 2 (spot 3 has a similar profile) and profile (c) corresponds to spot 1 (spot 4 has a similar profile) in (a). Normal force: 5.7 N.

The large plastic flow observed in the wear tracks (Fig. 4), the work hardening (Table 3), the build up of pronounced ridges (Figs. 3 and 4) and subsurface deformation structures (Figs. 7 and 8) indicate that the steel undergoes severe deformation during rubbing. In this situation, detachment of metallic particles is a consequence of breakdown of the metal laying underneath the boundary films by mechanisms such as low-cycle fatigue or

ratcheting. The presence of extruded strips of metal (Fig. 4a–c), partially exhibiting cracks, confirm the occurrence of wear by mechanical removal of metal particles. Surface films can affect the mechanical breakdown of metals surfaces by the so called Roscoe effect [4]. According to this, the observed results can thus be explained in the following way. In the wear track, Oil A generates a relatively hard iron oxide (Mohs hardness 5.5–6.6 [15], approximately 670–1000 HV) film on the steel surface while Oil B leads to the build-up of a soft calcium oxide (Mohs hardness 1.75 [15], approximately 50 HV) and calcium carbonate (Mohs hardness 3 [15], approximately 160 HV). The presence of the oxide hard film on the steel surface interferes with the dislocations generated by rubbing in two possible ways [17]: firstly, additional dislocations can be generated at the oxide/metal interface during deformation [18]. Secondly, the annihilation of dislocations generated underneath the surface by the contact stress field is inhibited by the hard film by blocking the emergence of slip bands on the surface [16]. As a consequence, dislocations and thus strain accumulations in the metal result in the observed larger work hardening (Table 3) and sensitivity to wear [6,9,17]. Further, the hard film can interfere with the deformation mechanisms of nano-crystalline metals that are supposed to proceed by grain rotation [10]. The hard adhering film can limit or even block such deformation mechanism. As a consequence nano-grains, which rotation is largely blocked, will tend to deform in the sliding direction to accommodate the plastic deformation. This hypothesis could explain the elongation of the surface grains observed in Oil A but not in Oil B (Fig. 8). The blocking of grain rotation introduces further strain into the metal and renders it more prone to breakdown. The additive package used in the preparation of Oil B suppresses the formation of the metal oxide film by producing a softer and thinner calcium rich surface film. Thus, in this case, less strain is accumulated in the metal and the rotation of nano-grains is not inhibited. As a consequence wear is significantly reduced.

Although the above deduced mechanistic interpretations need further assessment, the present work shows that also in oil lubricated contact, the formed boundary films do not act simply as friction reducers but also crucially affect the surface and subsurface mechanical and metallurgical response of metal and thus can significantly contribute in wear reduction.

5. Conclusions

In this study, the tribological performance of a steel ball-on-disc contact was evaluated in two commercial high-quality engine oils. Following conclusions could be drawn from this specific system:

- The two oils yielded after rubbing boundary films of different compositions: Oil A generated an iron–zinc oxide film covered by a calcium rich film. Oil B yielded a calcium rich film directly in contact with the metal without significant iron oxide formation.
- Friction was similar in the two oils while Oil A led to significantly larger wear than Oil B.
- The tribo-metallurgical response of the metal depends on the nature of the oil that was found to influence work hardening and yielded a more homogenous grain refined near surface metal layer.

As a general conclusion, this work has produced evidence that solid boundary films formed in oil lubricated systems can interfere with the plastic deformation response of the contacting steel and can significantly affect wear. This mechanical interaction was attributed to the mismatch in mechanical properties established at the metal/film interface that interferes with dislocation motion, work hardening, strain accumulation and finally wear particle generation. As a corollary, the development of high-performance oil additives could benefit from considering tribo-metallurgical effects of boundary films in addition to their intrinsic mechanical or lubricating properties.

Acknowledgments

The research was financially supported by the Swiss CTI project 17018.1 INNO-13-16-1W carried out in collaboration with Micro Tech Lubes SA, Geneva, Switzerland. The authors thank Pierre Mettraux for the SEM and XPS analysis. Shoufan Cao acknowledges grant from the China Scholarship Council.

References

[1] H. Spikes, The history and mechanisms of ZDDP, Tribol. Lett. 17 (2004) 469–489.
[2] A.J. Gellman, N.D. Spencer, Surface chemistry in tribology, Proc. Inst. Mech. Eng. Part J: J. Eng. Tribol. 216 (2002) 443–461.
[3] T. Kubo, S. Fujiwara, H. Nanao, I. Minami, S. Mori, TOF-SIMS analysis of boundary films derived from calcium sulfonates, Tribol. Lett. 23 (2006) 171–176.
[4] R. Roscoe, The plastic deformation of cadmium single-crystals, Philos. Mag. 21 (1936) 399–406.
[5] S. Mischler, A. Spiegel, D. Landolt, The role of passive oxide films on the degradation of steel in tribocorrosion systems, Wear 225–229 (1999) 1078–1087.
[6] A. Bidiville, M. Favero, P. Stadelmann, S. Mischler, Effect of surface chemistry on the mechanical response of metals in sliding tribocorrosion systems, Wear 263 (2007) 207–217.
[7] S. Guadalupe Maldonado, S. Mischler, M. Cantoni, W.J. Chitty, C. Falcand, D. Hertz, Mechanical and chemical mechanisms in the tribocorrosion of a Stellite type alloy, Wear 308 (2013) 213–221.
[8] N. Espallargas, S. Mischler, Tribocorrosion behaviour of overlay welded Ni–Cr 625 alloy in sulphuric and nitric acids: electrochemical and chemical effects, Tribol. Int. 43 (2010) 1209–1217.
[9] A. Igual Muñoz, N. Espallargas, Tribocorrosion mechanisms in sliding contacts, in: D. Landolt, S. Mischler (Eds.), Tribocorrosion of Passive Metals and Coatings, Woodhead Publishing, Cambridge, 2011, pp. 118–152.
[10] R. Büscher, A. Fischer, The pathways of dynamic recrystallization in all-metal hip joints, Wear 259 (2005) 887–897.
[11] J. Stojadinović, D. Bouvet, M. Declercq, S. Mischler, Effect of electrode potential on the tribocorrosion of tungsten, Tribol. Int. 42 (2009) 575–583.
[12] J. Stojadinovic, D. Bouvet, M. Declercq, S. Mischler, Influence of chelating agents on the tribocorrosion of tungsten in sulphuric acid solution, Electrochim. Acta 56 (2011) 7131–7140.
[13] J.F. Moulder, W.F. Stickle, P.E. Sobol, K.D. Bomben, Handbook of X-ray Photoelectron Spectroscopy, Physical Electronics Inc., Eden Prairie, 1995.
[14] ⟨http://srdata.nist.gov/xps/Default.aspx⟩, May 2016.
[15] ⟨http://www.newworldencyclopedia.org⟩, January 2016.
[16] T.Y. Zhang, C.F. Qian, Interaction of a screw dislocation with a thin-film-covered mode III crack, Acta Mater. 44 (1996) 4513–4520.
[17] J. Perret, E. Boehm-Courjault, M. Cantoni, S. Mischler, A. Beaudouin, W. Chitty, J.-P. Vernot, EBSD, SEM and FIB characterisation of subsurface deformation during tribocorrosion of stainless steel in sulphuric acid, Wear 269 (2010) 383–393.
[18] B. Viguier, Plasticity: recall the basic and microscopic aspects, in: B. Viguier (Ed.), Plastox 2007: Mechanisms and Mechanics of Plasticity–Environment Interactions, EDP Sciences, 2007, pp. 1–21.